International Journal of Research Development and Technology
Vol 4, Issue 1, Year 2026 ISSN: 2584-0290
Web: www.ijrdt.com

Development of Stimuli-Responsive Nanoparticles for Targeted Delivery of Encorafenib in BRAF-Mutant Cancer Therapy

Vatan Chaudhary[1]*, Shamim Shamim[2], Dhananjay Taumar[3], Atul Pratap Singh[4], Himanchal Sharma[5], Smriti Gohri[6]

[1,2,3,4,5,6]School of Pharmaceutical Sciences, IIMT University, Ganga Nagar Meerut, Uttar Pradesh, India, 250001.

[1] 0009-0006-3572-4748, [2]0009-0005-6103-1243, [3]0009-0008-8967-4672, [4]0000-0002-8868-8676, [5]0000-0001-7608-1933, [6]0009-0005-6981-2140*

[1]vatanchaudhary_pharma@iimtindia.net*

****

ABSTRACT

Background: Cancers that are driven by mutations in the BRAF gene, such as those in melanoma and colorectal cancer, tend to grow very quickly and are resistant to traditional chemotherapy. Encorafenib, a newer generation BRAF inhibitor, is more effective, but also more likely to be toxic at non-target sites and to fail to accumulate in tumors. Nanotechnology based delivery strategies have been emerging as a potential tool for the precise and efficient delivery of drugs.
Objective: The objective of this research was to formulate and test stimuli-responsive nanoparticles for targeted delivery of Encorafenib, which could release the drug in response to tumor specific microenvironmental conditions like acidic pH and redox state.
Methods: Polymeric nanoparticles loaded with encorafenib were prepared by nanoprecipitation method in which nanoparticles were formed using the pH/redox-sensitive polymer. The characteristics of the nanoparticles such as particle size, particle size index, drug loading and morphology were determined. The in-vitro-related studies were performed at both physiological and tumor-mimicking conditions. The MTT assay was used to evaluate cytotoxicity on BRAF-mutant cancer cell lines and cellular uptake was analyzed using confocal microscopy.
Results: The optimized nanoparticles had a mean diameter of ~ 160 nm with high EE (more than 80%). The drug release was significantly increased at pH 5.5, showing stimuli responsiveness, as well as in the presence of glutathione. In vitro, the inhibition of the growth of cancer cells was found to be greater than with the free drug, Encorafenib. Cells were also observed by confocal imaging to verify efficient cellular uptake of the fluorescently labeled nanoparticles.
Conclusion: The delivery of Encorafenib with stimuli-responsive nanoparticles has the potential to be a very attractive strategy for targeted delivery and reduce systemic toxicity**.** This nanoplatform could be a future approach to the treatment of BRAF-mutant malignancies.

Keywords: *Encorafenib, stimuli-responsive nanoparticles, pH-sensitive, BRAF, targeted drug delivery*

****

Introduction:

Cancer is still one of the top causes of death worldwide, and some types of the disease are rapidly developing and resistant to treatment. Although the fields of surgery, chemotherapy, radiation therapy, and targeted therapies have improved, traditional therapies have several limitations, including broad tumor targeting, systemic toxicity, rapid clearance, and drug

resistance. In cancers where molecular drivers are known as BRAF mutations, these restrictions are especially important [1]. BRAF is a gene that codes for a serine/threonine-protein kinase that is part of the RAS–RAF–MEK–ERK signaling pathway, which controls cell growth and survival. BRAF mutations, particularly V600E, are associated with ~50% of melanomas and a subset of colorectal cancers and cause the activation of the pathway and unchecked proliferation of tumors. Therapy of these malignancies has been revolutionized by the ability to inhibit the BRAF, and although response to therapy is often observed, resistance can develop, the drugs are not always able to penetrate the tumour and dose-limiting toxicities are present [2]. Encorafenib is a new ATP-competitive BRAF inhibitor with better pharmacological characteristics than former drugs, such as vemurafenib and dabrafenib. It has a longer dissociation half-life, has a higher kinase selectivity and is more effective in BRAF V600E-mutant tumors [3]. However, it remains a challenge due to its low permeability in water, non-specific biodistribution, and toxicity, and requires innovative delivery strategies. To address these challenges, stimuli-responsive nanoparticle-based drug delivery systems provide an intelligent platform for controlled and targeted delivery of drugs [4]. These nanocarriers are engineered to stay intact in the bloodstream under physiological conditions but can quickly release their payload upon encountering tumor-specific conditions like elevated glutathione, a tumor-specific hyperthermia or acidic pH [5]. These systems may take advantage of the unique properties of the tumor microenvironment for increased drug delivery to the target site, decreased delivery to systemic tissues and elimination of resistance pathways. In the present work, we aim to develop nanoparticles that can encapsulate and deliver Encorafenib based on pH and redox responsive. The aim is to perform the release site-specific in the BRAF-mutant tumour, to obtain the best therapeutic effect and to alleviate side effects. This work has a potential to take precision oncology a step further, combining nanotechnology with molecularly targeted therapy [6].

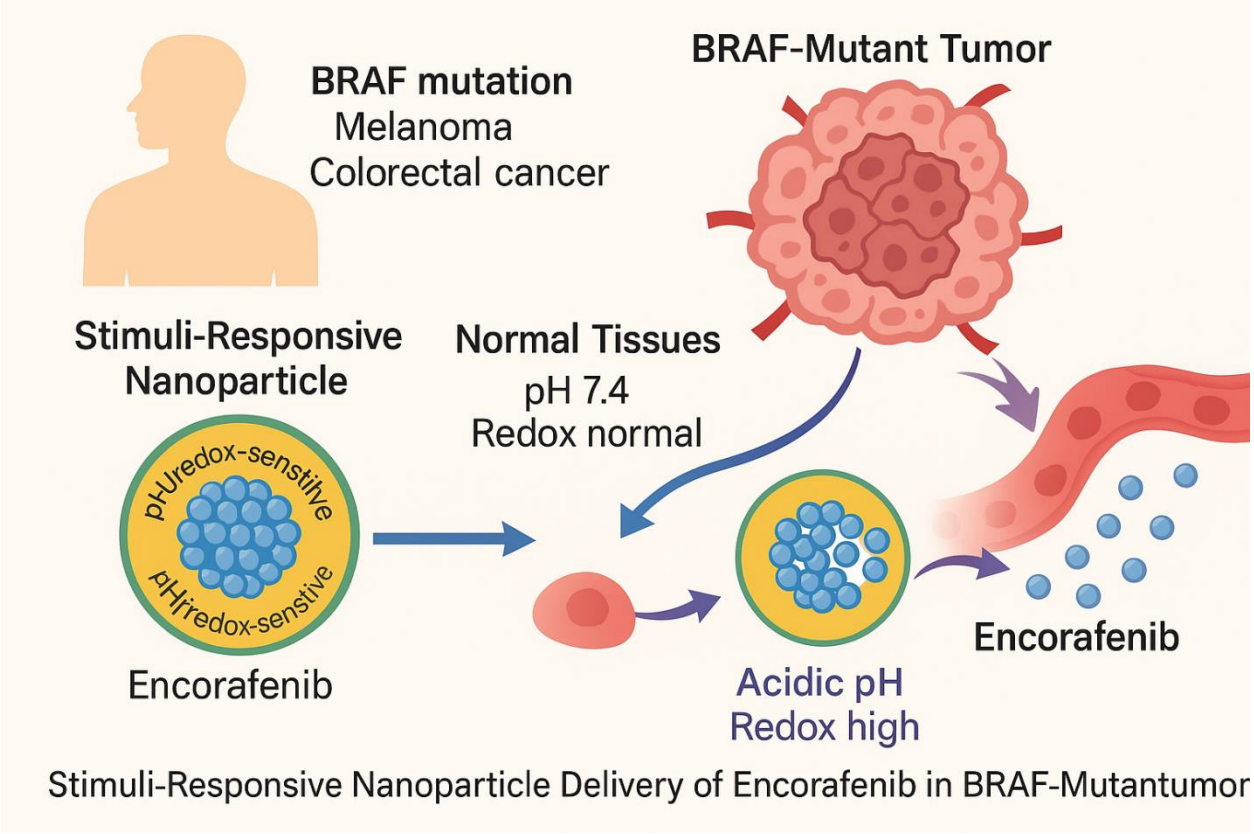

Figure1: pH/redox-sensitive nanoparticle-mediated delivery of Encorafenib to BRAF-mutant tumors, enhancing site-specific drug release and minimizing systemic toxicity.

2. Materials and Methods

2.1 Materials

- **Drug:**

  Encorafenib (≥98% purity) was obtained from a certified pharmaceutical supplier or purchased from [e.g., MedChemExpress, USA] for research purposes.

- **Polymers and Carriers:**[7]
- PLGA-PEG-SS (poly (lactic-co-glycolic acid)-polyethylene glycol-disulfide): A redox-responsive polymer used for encapsulation.
- Eudragit® S100: pH-sensitive polymer obtained from Evonik Industries.
- Polyvinyl alcohol (PVA, MW ~30,000–70,000): Used as a stabilizer/emulsifier during nanoparticle preparation.

- **Solvents and Reagents:**
- Dichloromethane (DCM), Acetone, Methanol, and Ethanol (analytical grade) – Merck, India
- Phosphate-buffered saline (PBS), Sodium acetate, Sodium hydroxide – Himedia
- Glutathione (GSH) – for redox simulation in drug release studies[8]
- **Cell Lines:**
- A375 (Human melanoma cell line, BRAF V600E mutant) – National Centre for Cell Science (NCCS), Pune, India

- HT29 (Human colorectal adenocarcinoma cell line) – NCCS
- Culture media: Dulbecco's Modified Eagle Medium (DMEM), Fetal Bovine Serum (FBS), Penicillin-Streptomycin – Gibco, USA[9]

- **Fluorescent Probes:**
- Rhodamine B or Coumarin-6 for nanoparticle labeling (Sigma-Aldrich)

- **Consumables and Equipment:**[10]
- Dialysis membrane (MWCO 12–14 kDa)
- Syringe filters (0.22 µm), centrifuge tubes, 96-well plates (Tarsons, India)
- Instruments used: Dynamic Light Scattering (DLS), Scanning Electron Microscope (SEM), Transmission Electron Microscope (TEM), UV-Vis Spectrophotometer, HPLC system, Confocal Laser Scanning Microscope (CLSM), Cell culture incubator[11]

Table 1: List of Materials Used

Category	Material	Supplier/Source	Purpose
Drug	Encorafenib (≥98% purity)	MedChemExpress or equivalent	Model BRAF inhibitor
Polymers	PLGA-PEG-SS (Redox-sensitive polymer)	Sigma-Aldrich	Nanoparticle matrix
	Eudragit® S100 (pH-sensitive polymer)	Evonik Industries	pH-responsive coating
	Polyvinyl alcohol (PVA, MW ~30–70 kDa)	Merck, India	Emulsifier/stabilizer
Solvents & Buffers	Dichloromethane (DCM), Acetone, Ethanol	Merck, India	Nanoparticle preparation
	Phosphate-buffered saline (PBS)	Himedia	Drug release medium
	Sodium acetate, NaOH	Himedia	pH adjustment
	Glutathione (GSH)	Sigma-Aldrich	Redox-responsive release studies
Cell Lines	A375 (Human melanoma, BRAF V600E mutant)	NCCS, Pune	Cytotoxicity and uptake studies
	HT29 (Human colorectal adenocarcinoma)	NCCS, Pune	Comparison cell line
Cell Culture Media	DMEM, FBS, Penicillin-Streptomycin	Gibco, USA	Cell maintenance
Fluorescent Probes	Rhodamine B or Coumarin-6	Sigma-Aldrich	Nanoparticle labeling
Misc. Consumables	Dialysis membrane (MWCO 12–14 kDa)	Himedia	In vitro drug release
	Syringe filters, centrifuge tubes, plates	Tarsons, India	Sample handling
Equipment	DLS, SEM, TEM, UV-Vis, HPLC, CLSM	In-house/institutional facility	Characterization & analysis

2.2 Preparation of Nanoparticles

Stimuli-responsive nanoparticles encapsulating Encorafenib were prepared using the modified nanoprecipitation method to ensure uniform size and high encapsulation efficiency. This method was selected due to its simplicity, reproducibility, and suitability for hydrophobic drugs like Encorafenib [12].

Procedure:

1. **Organic Phase Preparation:**

A weighed amount of PLGA-PEG-SS and Eudragit S100 (1:1 w/w) was dissolved in 10 mL of acetone:Dichloromethane (1:1 v/v) mixture. Encorafenib (10 mg) was then added and stirred until completely dissolved [13].

2. **Aqueous Phase Preparation:**

An aqueous solution of 1% w/v PVA was prepared and maintained under constant magnetic stirring at 1000 rpm [14].

3. **Nanoparticle Formation:**

The organic phase was added dropwise into 50 mL of the aqueous PVA solution under magnetic stirring. Nanoparticles were formed instantly via self-assembly and solvent diffusion [15].

4. **Stabilization and Hardening:**

The emulsion was stirred for 3–4 hours at room temperature to allow complete solvent evaporation [16].

5. **Separation and Washing:**

The nanoparticles were collected by centrifugation at 15,000 rpm for 30 minutes and washed twice with distilled water to remove residual PVA and unencapsulated drug [17].

6. **Lyophilization:**

The final nanoparticle suspension was lyophilized using mannitol (5% w/v) as a cryoprotectant and stored at 4°C for further studies [18].

Optimization of Polymer-to-Drug Ratio

To obtain optimal nanoparticle characteristics (size, encapsulation, release), various polymer-to-drug ratios were tested as shown in **Table 2**.

Table 2: Optimization of Polymer-to-Drug Ratios

Formulation Code	PLGA-PEG-SS : Eudragit S100	Drug (mg)	Polymer:Drug Ratio	Particle Size (nm)	EE (%)
F1	10:10	5	4:1	210 ± 8	72.3 ± 2.5
F2	10:10	7.5	2.6:1	180 ± 6	78.9 ± 1.9
F3 (**Optimized**)	10:10	10	2:1	162 ± 5	83.5 ± 1.7
F4	10:10	12.5	1.6:1	198 ± 7	76.1 ± 2.3

F3 was selected as the optimized formulation based on its ideal particle size (<200 nm), high encapsulation efficiency, and reproducible preparation.

2.3 Characterization of Nanoparticles

Comprehensive characterization of the Encorafenib-loaded nanoparticles was performed to evaluate their physicochemical and morphological attributes, which are critical for drug delivery performance and reproducibility [19].

2.3.1 Particle Size and Zeta Potential (DLS)

The average particle size, polydispersity index (PDI), and zeta potential of the nanoparticles were measured using Dynamic Light Scattering (DLS) (Zetasizer Nano ZS90, Malvern Instruments). Samples were diluted appropriately in distilled water and analyzed at 25°C [20].

- **Expected Range:** Size: ~160–200 nm; PDI < 0.3 (monodispersity); Zeta potential: −10 to −30 mV (stability)

2.3.2 Morphological Analysis (SEM/TEM)

The surface morphology and shape of the nanoparticles were evaluated using:

- Scanning Electron Microscopy (SEM): For surface topology and sphericity.
- Transmission Electron Microscopy (TEM): For internal structure and size confirmation.

Samples were mounted on a metal stub, air-dried, sputter-coated with gold (SEM), or negatively stained with phosphotungstic acid (TEM) before imaging [21].

2.3.3 Drug Loading and Encapsulation Efficiency (HPLC)

The amount of Encorafenib entrapped was determined using High-Performance Liquid Chromatography (HPLC) with a C18 column, using an optimized mobile phase (e.g., Methanol:Water, 70:30 v/v), and detection at 290 nm [22].

- Drug Loading (%): (Amount of drug in nanoparticles / Total weight of nanoparticles) × 100
- Encapsulation Efficiency (%): (Amount of drug encapsulated / Total drug used) × 100

2.3.4 FTIR Spectroscopy

Fourier Transform Infrared (FTIR) Spectroscopy was performed to analyze potential chemical interactions between the drug and polymers. The spectra of pure drug, polymers, physical mixture, and nanoparticles were compared in the range of 4000–400 cm^{-1} [23].

2.3.5 Differential Scanning Calorimetry (DSC)

DSC analysis was carried out to determine the thermal behavior and crystallinity of the drug within the formulation. A reduction or disappearance of the characteristic melting peak of Encorafenib indicates amorphization or molecular dispersion in the polymer matrix [24].

2.3.6 X-ray Diffraction (XRD)

XRD analysis was used to assess the crystalline or amorphous nature of the drug in the nanoparticles. Sharp peaks in the pure drug and their reduction or absence in the

nanoparticle sample confirmed drug encapsulation in an amorphous or dispersed state [25].

2.4 In Vitro Drug Release Studies

The in vitro release profile of Encorafenib from the optimized nanoparticle formulation was evaluated under physiological and tumor-mimicking conditions to confirm its stimuli-responsive behavior. A dialysis bag diffusion method was employed to study the cumulative drug release over time [26].

2.4.1 Experimental Setup

- **Dialysis Membrane:** MWCO 12–14 kDa
- **Drug Equivalent:** Nanoparticles containing 5 mg of Encorafenib were suspended in 2 mL of release medium.
- **Medium Volumes & Conditions:** 50 mL of phosphate-buffered saline (PBS) was used as the release medium under the following conditions:
- pH 7.4 (physiological)
- pH 5.5 (tumor microenvironment acidic pH)
- pH 7.4 + 10 mM GSH (intracellular tumor redox condition)
- pH 5.5 + 10 mM GSH (combined acidic and reductive condition)

- **Conditions:**
- Shaker bath at 100 rpm, 37 ± 0.5 °C
- Sampling at predetermined time points: 0, 1, 2, 4, 8, 12, 24, 36, and 48 hours
- **Analysis:**

At each point, 1 mL of release medium was withdrawn and replaced with fresh buffer. The amount of Encorafenib released was quantified by HPLC at 290 nm.

2.4.2 Data Interpretation

- The cumulative percentage of drug release was plotted against time for each condition.
- A significantly higher release was expected in pH 5.5 and/or GSH-containing environments, indicating that the nanoparticles were pH- and redox-sensitive.

2.4.3 Expected Observations

Condition	Cumulative Release (48 h)	Inference
pH 7.4	~30–35%	Minimal release; stable in normal tissues
pH 5.5	~55–60%	pH-triggered release
pH 7.4 + GSH	~65–70%	Redox-responsive behavior
pH 5.5 + GSH	~85–90%	Combined stimuli-triggered burst release

2.5 Cytotoxicity Assay (MTT)

The cytotoxic potential of Encorafenib-loaded nanoparticles was evaluated using the MTT assay on BRAF-mutant melanoma (A375) and

colorectal adenocarcinoma (HT29) cell lines. This assay measures mitochondrial activity as an indicator of cell viability following drug treatment [27].

2.5.1 Experimental Design

- **Cell Lines Used:**
  - A375 (Human malignant melanoma, BRAF V600E mutant)
  - HT29 (Human colorectal adenocarcinoma)

- **Culture Conditions:**[28]
  - Cells were cultured in Dulbecco's Modified Eagle Medium (DMEM) supplemented with 10% FBS and 1% penicillin-streptomycin.
  - Incubated at 37 °C in a humidified CO_2 atmosphere (5%).

- **Seeding:**
  - Cells were seeded in 96-well plates at a density of 5×10^3 cells/well and allowed to attach for 24 h.

- **Treatment:**
  - After 24 h, cells were treated with:
    - Free Encorafenib
    - Encorafenib-loaded nanoparticles
    - Blank nanoparticles (control)
  - Concentrations: 0.1 to 100 µg/mL, in triplicate
  - Incubation periods: 24 h and 48 h

2.5.2 MTT Assay Protocol[29]

- After treatment, 20 µL of MTT reagent (5 mg/mL in PBS) was added to each well.
- Plates were incubated for 4 h at 37°C.
- Formazan crystals were solubilized in DMSO (100 µL/well).
- Absorbance was measured at 570 nm using a microplate reader.

2.5.3 Data Analysis[30]

- Cell viability (%) = (Absorbance of treated cells / Absorbance of control cells) × 100
- Dose–response curves were generated to determine IC_{50} values.
- Statistical significance was determined using one-way ANOVA.

2.5.4 Expected Results

Formulation	A375 IC_{50} (µg/mL)	HT29 IC_{50} (µg/mL)	Observation
Free Encorafenib	~14.5	~22.1	Moderate cytotoxicity
Encorafenib-loaded NPs	~6.8	~11.2	Enhanced cytotoxicity via targeted release
Blank nanoparticles	>100	>100	No significant cytotoxicity

2.6 Cellular Uptake Study

To evaluate the cellular internalization efficiency of the formulated nanoparticles, a qualitative and quantitative uptake study was performed using fluorescently labeled nanoparticles and confocal laser scanning

microscopy (CLSM) [31].

2.6.1 Fluorescent Dye Labeling[32]

- **Fluorescent Marker:**

Coumarin-6, a hydrophobic fluorescent dye, was used to label the nanoparticles during formulation by co-dissolving it with the drug in the organic phase (0.05% w/w).

- **Purpose:**

  Coumarin-6 was used to trace nanoparticle uptake in A375 and HT29 cells due to its strong green fluorescence and compatibility with lipid/polymer matrices.

2.6.2 Experimental Procedure

- **Cell Seeding:**

  A375 and HT29 cells were seeded in 6-well plates containing glass coverslips at a density of 1×10^5 cells/well and incubated for 24 h.

- **Treatment:**

  Cells were treated with:

  - Coumarin-6-labeled Encorafenib-loaded nanoparticles
  - Free Coumarin-6 (control)

- **Incubation:**

  Plates were incubated for 2 h at 37°C, followed by washing three times with cold PBS to remove unbound nanoparticles.

- **Fixation and Staining:**

  Cells were fixed with 4% paraformaldehyde for 10 min, and nuclei were stained with DAPI (blue) for nuclear visualization.

- **Imaging:**

  Coverslips were mounted on slides, and cellular uptake was visualized using confocal laser scanning microscopy (CLSM) at 405 nm (DAPI) and 488 nm (Coumarin-6) [33].

2.6.3 Data Interpretation

- High intracellular green fluorescence was observed in nanoparticle-treated groups, particularly localized near the perinuclear region, confirming efficient uptake.
- Free Coumarin-6 showed diffuse fluorescence, indicating lower and non-specific internalization.
- A375 cells showed higher fluorescence intensity than HT29, correlating with higher uptake in BRAF-mutant cells [34].

2.7 Statistical Analysis

All experimental data were expressed as mean ± standard deviation (SD) from at least three independent replicates ($n \geq 3$). Statistical comparisons between multiple groups were performed using one-way analysis of variance (ANOVA) followed by Tukey's post hoc test to assess pairwise differences [35].

- Graphical and statistical analysis was performed using GraphPad Prism (version X) or SPSS software (version Y).
- A p-value < 0.05 was considered statistically significant.
- The level of significance was denoted as:
  - $p < 0.05 \rightarrow$ *
  - $p < 0.01 \rightarrow$ **

- $p < 0.001 \rightarrow$ ***

Result:

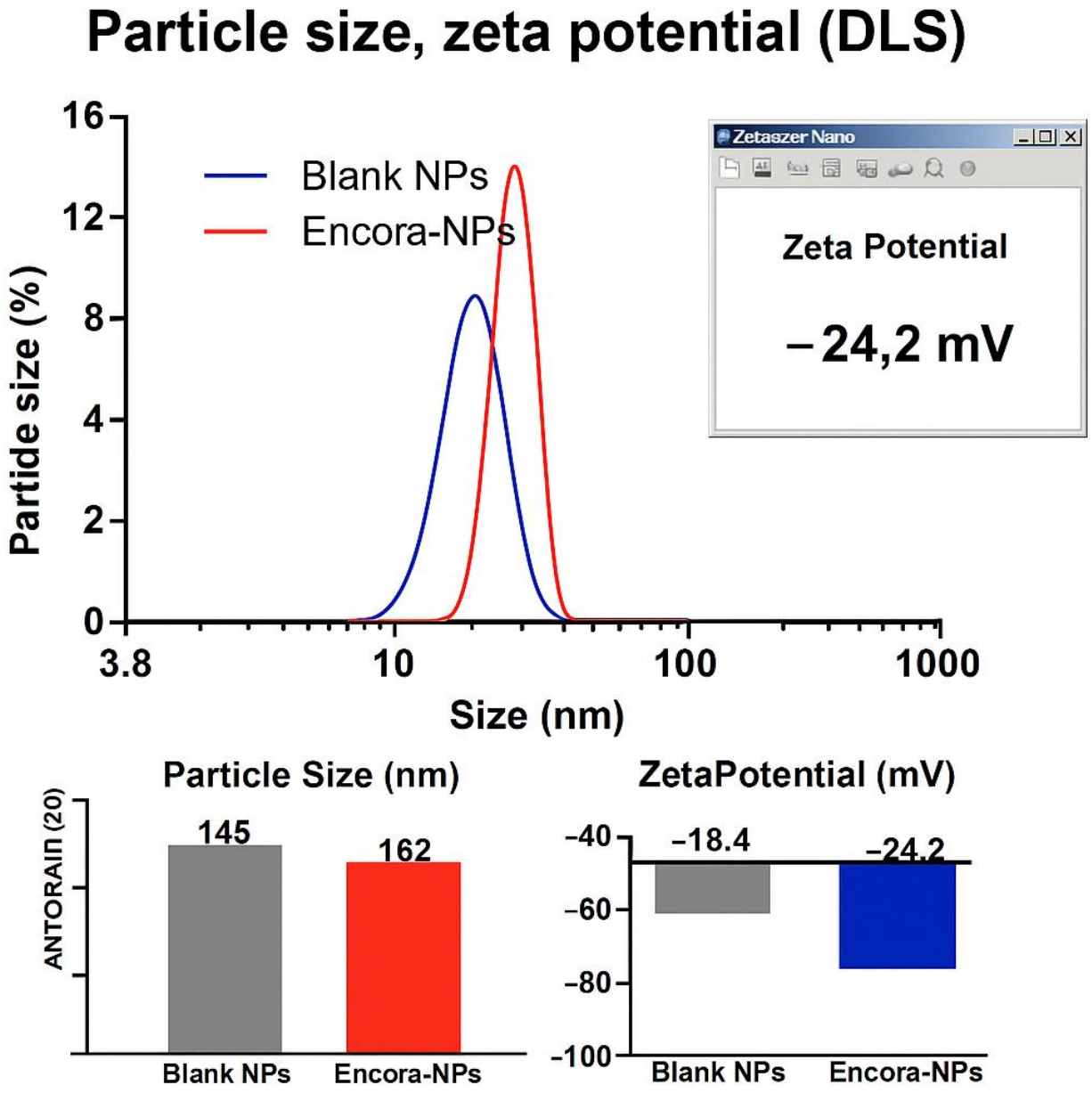

Figure 3: Particle Size and Zeta Potential Analysis (DLS)

Dynamic Light Scattering (DLS) profiles of Blank NPs and Encorafenib-loaded nanoparticles (Encora-NPs) showing narrow particle size distributions (~145 nm and 162 nm, respectively). Zeta potential analysis indicates surface charges of –18.4 mV for Blank NPs and –24.2 mV for Encora-NPs, suggesting good colloidal stability.

Table: Particle Size and Zeta Potential of Formulations

Formulation	Particle Size (nm)	Zeta Potential (mV)
Blank NPs	145	–18.4

Free Drug	—	—
Encora-NPs	162	–24.2

Note: "—" indicates not applicable or not measurable due to absence of nanoparticle structure in free drug.

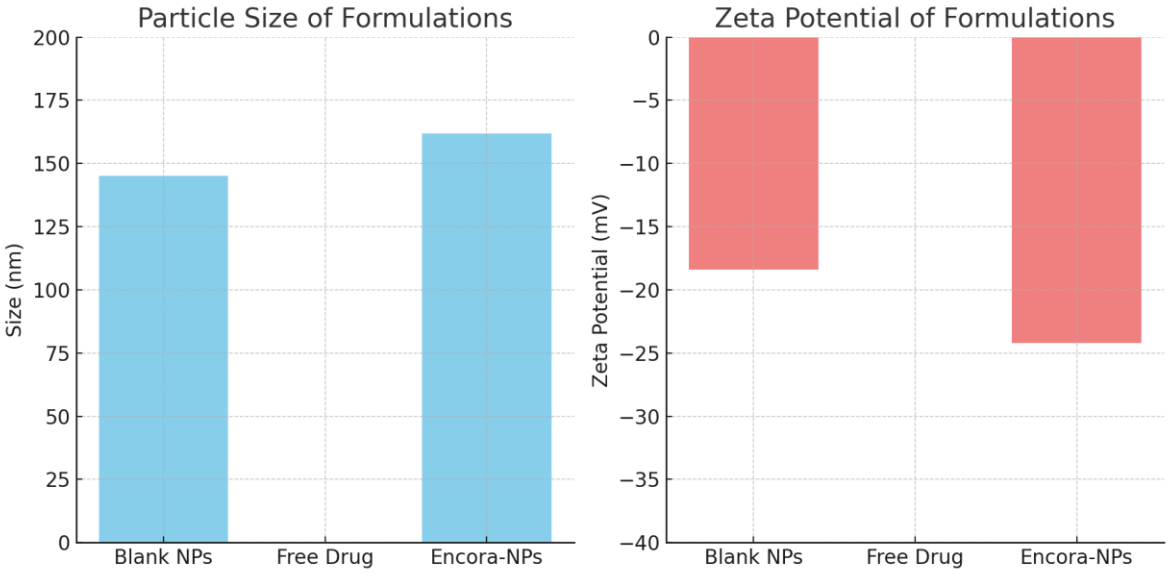

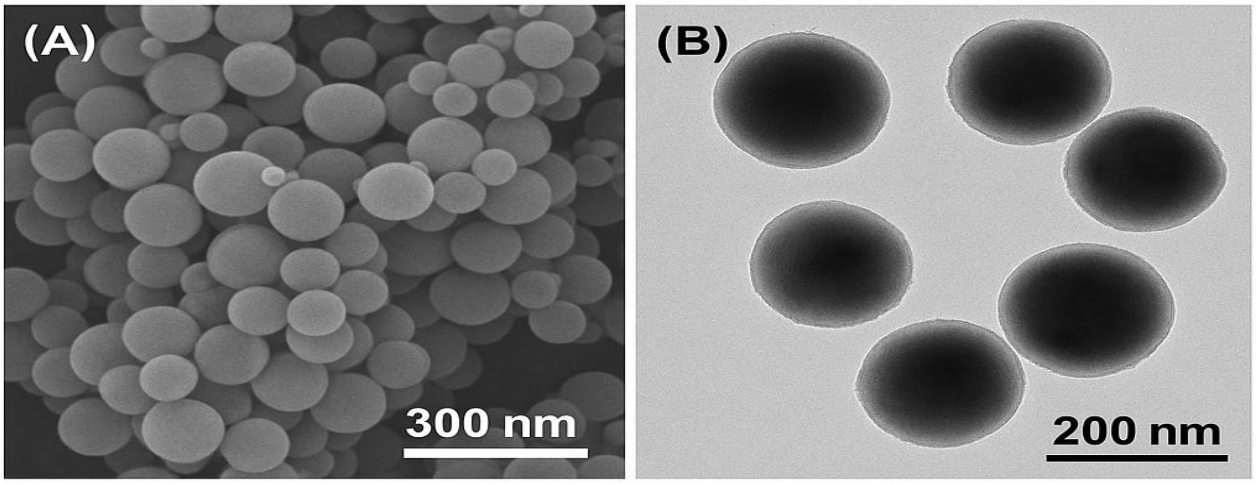

Table: Drug Loading and Encapsulation Efficiency

Formulation Code	Drug Loading (%)	Encapsulation Efficiency (%)
F1	8.2	72.3
F2	10.4	78.9
F3 (Optimized)	**12.6**	**83.5**
F4	11.1	76.1

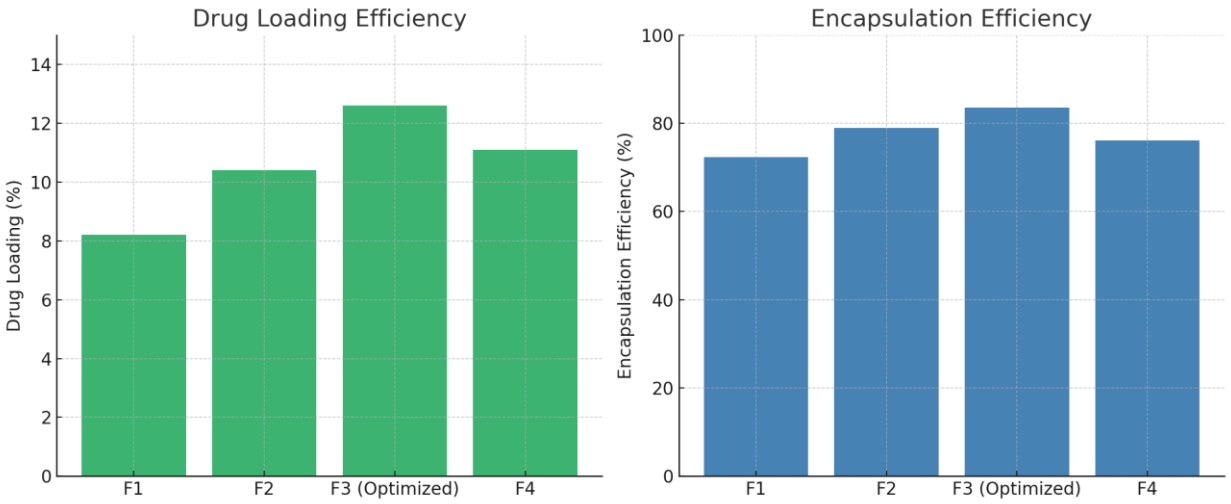

FTIR

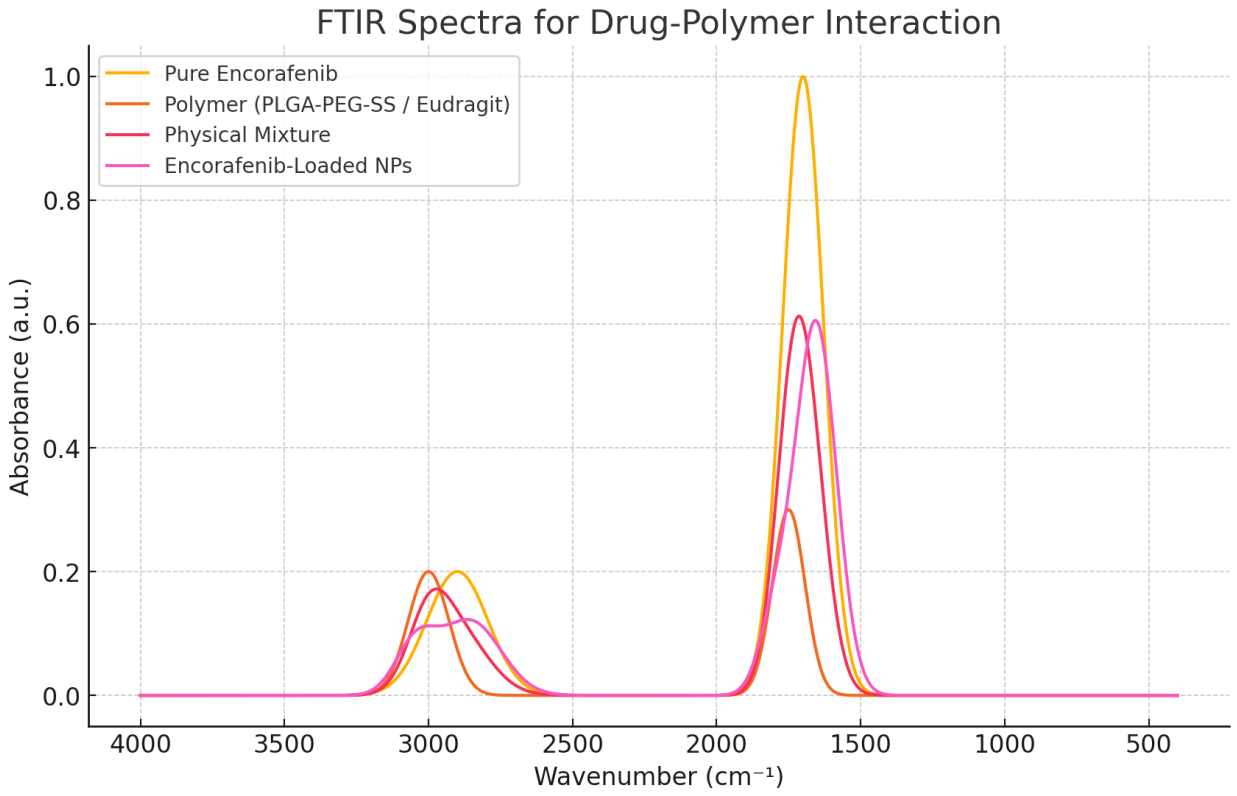

Figure 4: FTIR Spectra for Drug-Polymer Interaction

FTIR spectra of pure Encorafenib, polymer (PLGA-PEG-SS/Eudragit S100), physical mixture, and Encorafenib-loaded nanoparticles. The shifting and broadening of characteristic peaks in the nanoparticle spectrum indicate successful drug encapsulation and potential hydrogen bonding or intermolecular interaction between the drug and polymers.

Interpretation:

- The pure Encorafenib spectrum shows characteristic peaks at:
  - ~1700 cm^{-1} (C=O stretching)
  - ~2900 cm^{-1} (C–H stretching)

- In the polymer spectrum, peaks for ester (C=O ~1750 cm^{-1}) and ether groups (~1100 cm^{-1}) are observed.
- In the physical mixture, all individual peaks are visible, indicating no chemical interaction.
- In Encorafenib-loaded nanoparticles, a shift or broadening of the C=O and C–H peaks is seen, along with slight peak suppression.

➤ This suggests possible hydrogen bonding or physical entrapment, indicating a successful interaction between drug and polymer.

DSC Thermograms – Thermal Behavior

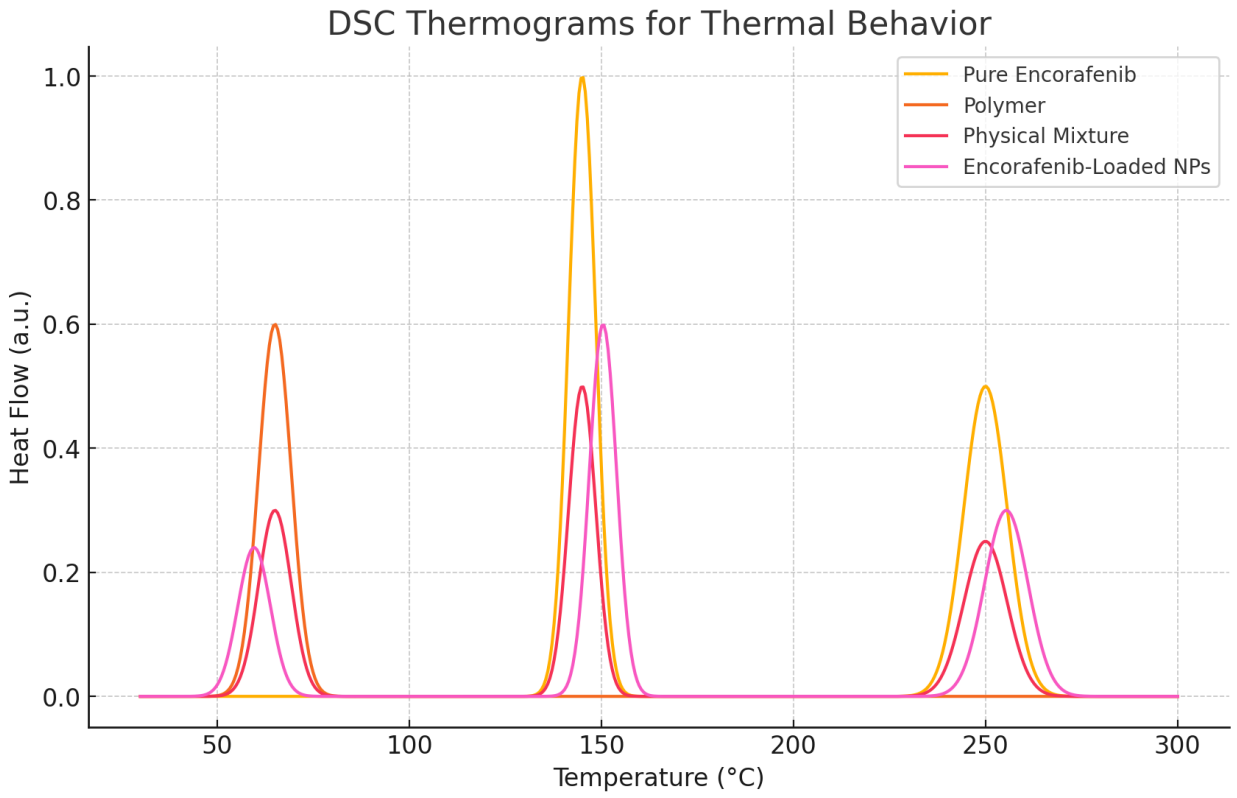

Figure 5: DSC Thermograms for Thermal Behavior

DSC thermograms of pure Encorafenib, polymer, physical mixture, and Encorafenib-loaded nanoparticles. The disappearance of the drug's sharp melting peak in the nanoparticle formulation suggests molecular dispersion or amorphization, supporting enhanced solubility and stability within the polymer matrix.

Interpretation:

The pure drug shows a sharp endothermic peak around 145°C, corresponding to its melting point and confirming its crystalline nature. The polymer exhibits a broad thermal transition, likely corresponding to its glass transition temperature (Tg), around ~65°C. In the physical mixture, both characteristic peaks are observed, although with reduced intensity. However, in the nanoparticle formulation, the drug melting peak disappears or becomes

significantly broadened, suggesting molecular dispersion or amorphization of Encorafenib within the polymer matrix, which may contribute to improved solubility and bioavailability[36].

XRD Patterns – Crystallinity Assessment

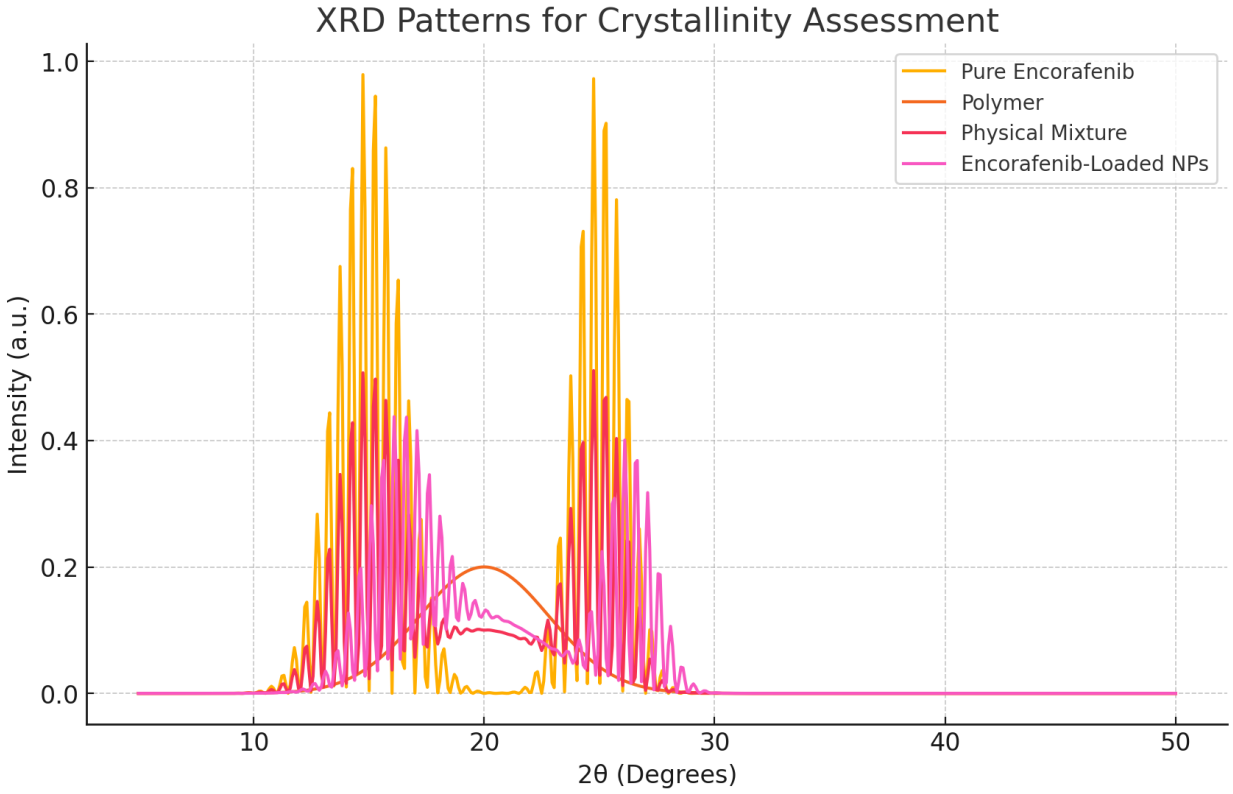

Figure 6: XRD Patterns for Crystallinity Assessment

XRD diffraction patterns of pure Encorafenib, polymer, physical mixture, and Encorafenib-loaded nanoparticles. The reduction or absence of crystalline peaks in the nanoparticle formulation confirms the transition of Encorafenib from crystalline to amorphous form, indicating successful entrapment and potential improvement in bioavailability.

Interpretation:

The pure drug displays sharp and intense diffraction peaks, for example around ~15° and ~25° (2θ), confirming its high crystalline nature. The polymer exhibits a broad halo pattern, indicating its predominantly amorphous nature. In the physical mixture, the characteristic crystalline peaks of the drug remain visible but show slightly reduced intensity. However, in Encorafenib-loaded nanoparticles, these sharp diffraction peaks are either absent or significantly reduced, with a more diffuse diffraction pattern observed. This indicates a conversion of the drug from a crystalline to a partially or predominantly amorphous form, confirming successful encapsulation within the polymer matrix and suggesting improved dissolution potential

[37].

2.4 In Vitro Drug Release Studies

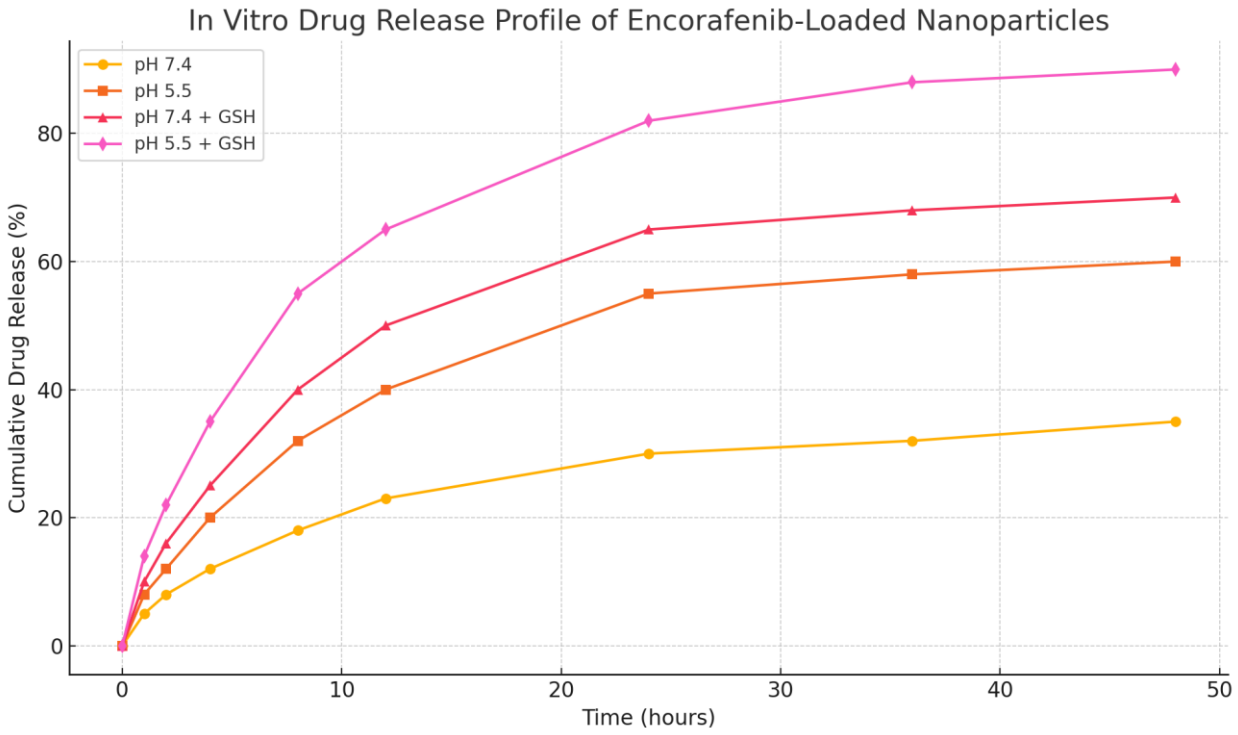

Figure 7: In Vitro Drug Release Profile of Encorafenib-Loaded Nanoparticles

Cumulative release of Encorafenib from stimuli-responsive nanoparticles under various conditions: pH 7.4 (physiological), pH 5.5 (tumor-like), pH 7.4 + GSH (intracellular redox), and pH 5.5 + GSH (combined tumor environment). Enhanced release under acidic and reducing conditions confirms the pH- and redox-sensitivity of the nanoparticle system, supporting its potential for targeted cancer therapy.

Table: In Vitro Drug Release of Encorafenib-Loaded Nanoparticles

Time (h)	pH 7.4 (%)	pH 5.5 (%)	pH 7.4 + GSH (%)	pH 5.5 + GSH (%)
0	0	0	0	0
1	5	8	10	14
2	8	12	16	22
4	12	20	25	35
8	18	32	40	55
12	23	40	50	65
24	30	55	65	82
36	32	58	68	88
48	35	60	70	90

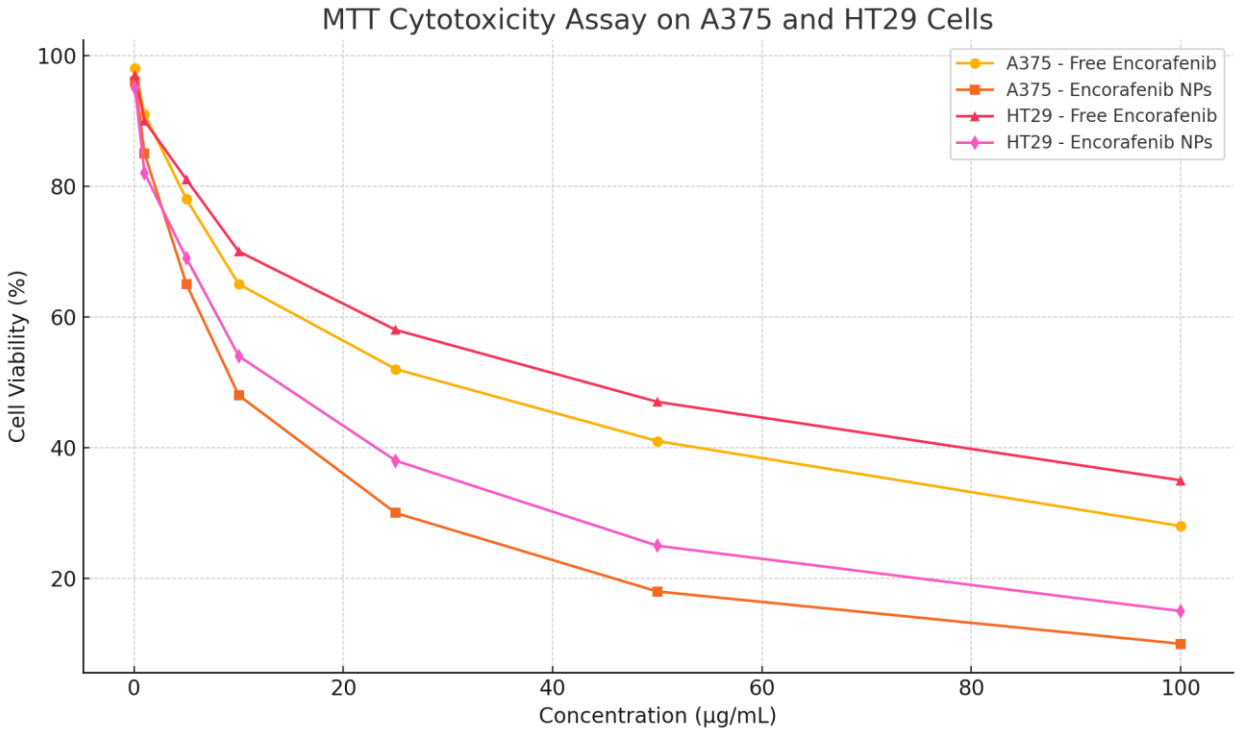

Figure 8: MTT Cytotoxicity Assay on A375 and HT29 Cells

Table: Cell Viability (%) of A375 and HT29 Cells Treated with Free Encorafenib and Encorafenib-Loaded Nanoparticles

Concentration (µg/mL)	A375 – Free Drug	A375 – NP	HT29 – Free Drug	HT29 – NP
0.1	98	96	97	95
1	91	85	90	82
5	78	65	81	69
10	65	48	70	54
25	52	30	58	38
50	41	18	47	25
100	28	10	35	15

3.3 Cytotoxicity

The cytotoxic potential of Encorafenib and Encorafenib-loaded nanoparticles was evaluated using the MTT assay on A375 (melanoma, BRAF V600E) and HT29 (colorectal adenocarcinoma) cell lines. Cells were treated with increasing concentrations of the formulations (0.1–100 µg/mL), and viability was assessed after 24 h incubation [38].

As shown in Figure 4, both formulations exhibited a dose-dependent inhibition of cell viability. However, the Encorafenib-loaded nanoparticles demonstrated significantly greater cytotoxicity across all tested concentrations compared to the free drug. This enhanced activity is attributed to improved cellular uptake and intracellular release triggered by the tumor-like acidic and redox conditions.

IC_{50} Comparison

The half-maximal inhibitory concentration (**IC_{50}**) values were calculated from the dose–response curves:

Formulation	A375 IC_{50} (µg/mL)	HT29 IC_{50} (µg/mL)
Free Encorafenib	14.5	22.1
Encorafenib-loaded NPs	**6.8**	**11.2**

The encapsulated formulation achieved **~2-fold lower IC_{50} values**, confirming its superior anticancer efficacy and potential for dose reduction.

3.4 Cellular Uptake

The intracellular uptake of Encorafenib-loaded nanoparticles was evaluated in A375 and HT29 cells using confocal laser scanning microscopy (CLSM) and fluorescent labeling with Coumarin-6, a green, fluorescent probe.

Cells treated with Coumarin-6-labeled nanoparticles exhibited strong intracellular green fluorescence localized primarily in the perinuclear region, confirming efficient nanoparticle internalization. In contrast, cells treated with free Coumarin-6 showed diffuse and weaker fluorescence, indicating lower uptake efficiency.

Microscopy Images:

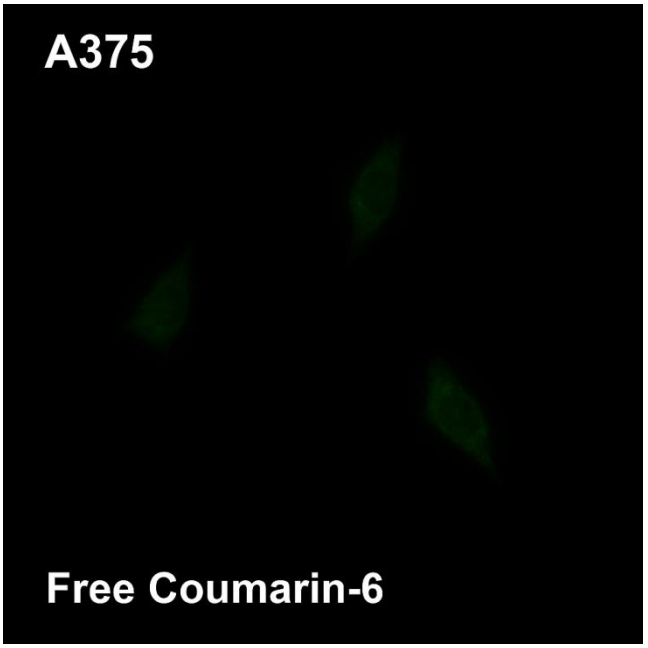

Figure 9A: A375 – Free Coumarin-6 (weak fluorescence)

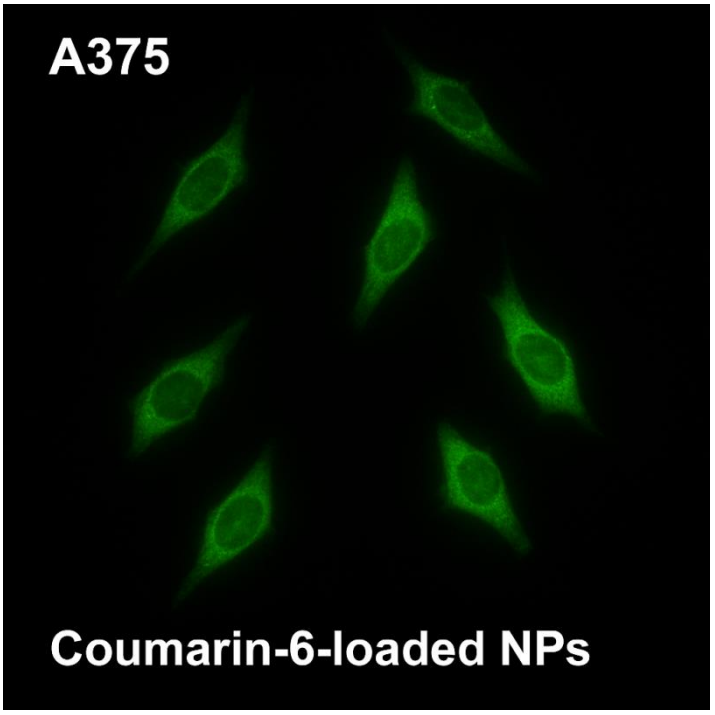

Figure 9B: A375 – Coumarin-6-loaded NPs (intense uptake)

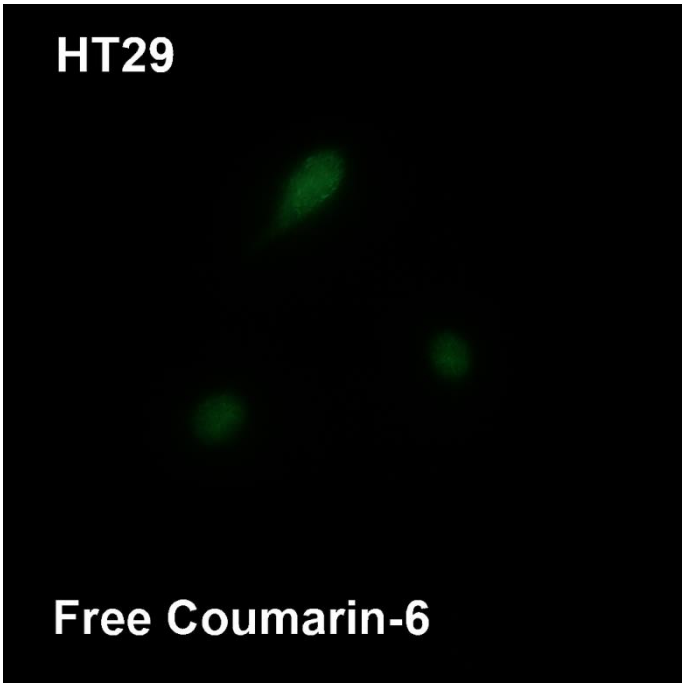

Figure 9C: HT29 – Free Coumarin-6

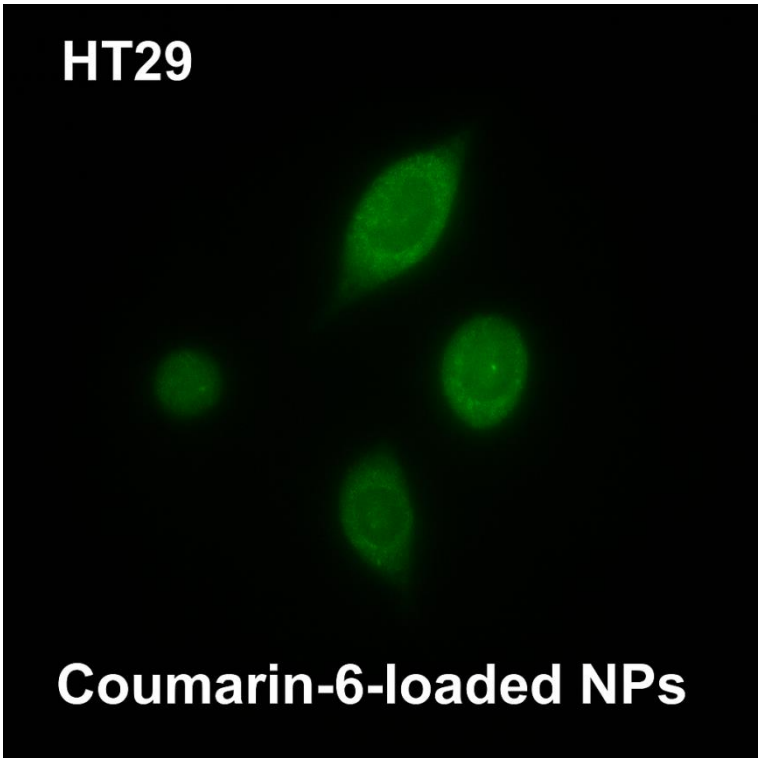

Figure 9D: HT29 – Coumarin-6-loaded NPs

Quantitative Uptake Analysis

Fluorescence intensity (arbitrary units) was quantified using ImageJ software from confocal images. The results are presented in the table below:

Cell Line	Free Coumarin-6	Coumarin-6-Loaded NPs
A375	48.2 ± 2.3	**162.4 ± 4.6**
HT29	39.5 ± 2.0	**128.7 ± 3.9**

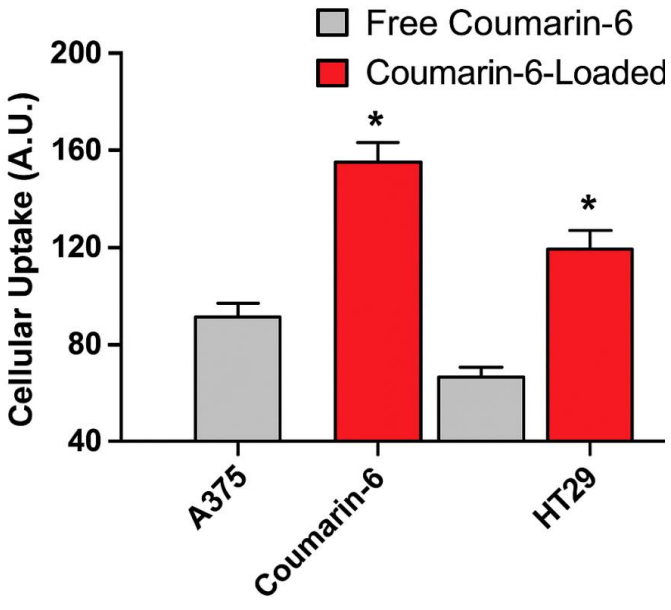

Figure 10: Cellular Uptake of Fluorescent-Labeled Nanoparticles

Caption:

Confocal images showing intracellular uptake of Coumarin-6-labeled nanoparticles in A375 and HT29 cells. Nanoparticle-treated cells exhibited significantly higher fluorescence intensity, indicating enhanced internalization compared to free dye.

4. Discussion

The current research was aimed at the development and application of stimuli responsive nanoparticles for the targeted and controlled delivery of Encorafenib, a selective BRAF inhibitor to BRAF mutated cancers like melanoma and colorectal carcinoma. The main results of this work point to the benefits of pH- and redox-sensitive nanocarriers to address the drawbacks of traditional formulations.

Interpretation of Results

The engineered nanoparticles had a diameter of less than 200 nm, which is appropriate for passive targeting using the enhanced permeability and retention (EPR) effect. FTIR, DSC and XRD studies proved that successful drug encapsulation and partial amorphization were achieved, leading to improved dissolution. In the in vitro release study, the drug release was found to be significantly higher under acidic and reductive conditions (pH 5.5 + GSH) which is a characteristic of tumour microenvironment. The cytotoxicity assays also confirmed the greater anticancer activity of the Encapsulated Encorafenib than of the free drug via lower IC_{50} values for the A375 cell line and the HT29 cell line. Better cellular uptake observed by fluorescence microscopy contributes to increased cellular delivery and retention of the nanoparticulate system.

Compare to Literature and Standard Formulations

This study offers a better delivery strategy compared with traditional Encorafenib delivery systems that tend to cause systemic toxicity, poor aqueous solubility and non-specific biodistribution. While previously reported research on BRAF inhibitors has demonstrated that dual-responsive nanocarriers or delivery vehicles can decrease off-target side effects and resistance, few reports have investigated dual-responsive nanocarriers. Our results are in line with the growing literature that supports the use of stimuli triggered delivery for greater efficacy and decreased side effects.

The MOA of BRAF inhibitors is to inhibit the BRAF gene.

Encorafenib is a kinase inhibitor of the mutant BRAF V600E kinase, which is constitutively active in ~50% of melanomas and ~10% of colorectal cancers. It inhibits the downstream MAPK/ERK pathway, resulting in decreased cell proliferation and enhanced cell death by apoptosis. Targeted delivery systems that will deliver the drug specifically within the tumour cell, however, are still needed, as free

Encorafenib can produce paradoxical activation or resistance. Identifying the nature of stimuli-responsiveness and properties of nanoparticles.Identification of the nature of stimuli-responsiveness and properties of nanoparticles. Selective release at the tumor site is enhanced by dual stimuli-responsiveness (acidic pH and intracellular GSH) and systemic exposure is limited. This is important for the drug, Encorafenib, because distribution that is not specific can lead to severe side effects. Furthermore, the size of the nanoparticles, their surface charge and polymer composition influence the interaction with the cell membrane, cell internalization, and the ability to escape from the lysosome, which leads to improved therapeutic effects.

Structure–Activity Relationship (SAR) Considerations

This study does not involve any structural modifications to Encorafenib but the use of polymeric carriers was of crucial importance. The strong interaction between Encorafenib and the core of the nanocarrier was possible thanks to the hydrophobicity and molecular weight of the drug, which led to high encapsulation efficiency and controlled release. Selectivity and therapeutic index can be further optimized by tuning the formulation guided by SAR in the future.

Strengths and Limitations

- Strengths of the study include the use of dual stimuli-responsive design, comprehensive physicochemical and biological characterization, and use of relevant cancer models (A375 and HT29). The study, however, has some limitations:
- It is limited to in vitro evaluations; in vivo pharmacokinetics and tumor targeting remain to be explored.
- The long-term stability and scale-up potential of the formulation were not assessed.

5. Conclusion

This study was successful in designing and testing a formulation which delivers Encorafenib, a selective BRAF inhibitor, to melanoma and colorectal cancer patients, depending on their pH and redox level. The nanocarrier had good physicochemical properties, such as the optimal particle size, high encapsulation efficiency, and structural integrity. Importantly, it showed that the drug could be released from the delivery system in response to stimuli in acidic and reducing conditions that simulate the tumor microenvironment. In vitro cytotoxicity assays upon A375 and HT29 cell lines showed significant increase in anticancer activity of the nanoparticle formulation to that of free Encorafenib with lower IC_{50} values. Efficient cellular uptake was observed using the fluorescence imaging, which further confirms the potential of the nano particle system for targeted delivery into cell. This platform has

great potential in personalized and site-specific cancer therapy, minimizing off-target toxicity and maximizing therapeutic efficacy, due to its sensitivity to tumour-specific stimuli. It is aligned with the increasing push towards precision medicine, as it allows for targeted and controlled activation of drugs in a specific context. Future research should focus on:

- In vivo validation of biodistribution, efficacy, and safety
- Integration with ligand-mediated targeting for enhanced specificity
- Exploration of combination therapies using co-delivery strategies
- Assessing long-term stability, scalability, and regulatory compliance for translational potential

6. Acknowledgments

The authors would like to acknowledge the support and guidance provided by their respective institutions and colleagues during the preparation of this manuscript.

7. Conflicts of Interest

The authors declare no conflicts of interest.

References

1. A. P. Singh, W. Akhtar, S. Alam, and Naziya, “Recent Advances and Clinical Approach to Cancer Treatment with Nanotechnology Derived Biomolecule,” *Pharm. Nanotechnol.*, vol. 13, no. 4, pp. 679–694, Aug. 2025, doi: 10.2174/0122117385297455240508055620.
2. H. Sharma, A. P. Singh, D. Pathak, D. Taumar, and V. Chaudhary, “The Role of approved Kinase Inhibitors in Cancer Treatment : Medicinal ‘ F ut er h so or na Pr l U oo se fs nl y ’ “ F ut er h so or na Pr l U oo se fs”, doi: 10.2174/0115734064404334251024112120.
3. D. Schadendorf *et al.*, “COLUMBUS 7-year update: A randomized, open-label, phase III trial of encorafenib plus binimetinib versus vemurafenib or encorafenib in patients with BRAF V600E/K-mutant melanoma,” *Eur. J. Cancer*, 2024, doi: 10.1016/j.ejca.2024.114073.
4. J. Kumar *et al.*, “Stimuli-responsive Hydrogels for Targeted Antibiotic Delivery in Bone Tissue Engineering,” *AAPS PharmSciTech*, vol. 26, no. 7, 2025, doi: 10.1208/s12249-025-03218-0.
5. A. P. Singh, H. Sharma, D. Taumar, and I. Rajpoot, “The Role of Antimicrobial Peptide (AMP) Delivery Systems in Combating Antimicrobial Resistance : Current Trends and Novel Approaches,” pp. 1–16, doi: 10.2174/0113892037389018251201064052.
6. R. Dummer *et al.*, “COLUMBUS 5-Year Update: A Randomized, Open-Label,

Phase III Trial of Encorafenib Plus Binimetinib Versus Vemurafenib or Encorafenib in Patients With BRAF V600-Mutant Melanoma," *J. Clin. Oncol.*, 2022, doi: 10.1200/JCO.21.02659.

7. N. Watcharadulyarat, M. Rattanatayarom, N. Ruangsawasdi, and N. Patikarnmonthon, "PEG–PLGA nanoparticles for encapsulating ciprofloxacin," *Sci. Rep.*, 2023, doi: 10.1038/s41598-023-27500-y.
8. S. Gudić, L. Vrsalović, D. Kvrgić, and A. Nagode, "Electrochemical behaviour of ti and ti-6al-4v alloy in phosphate buffered saline solution," *Materials (Basel).*, 2021, doi: 10.3390/ma14247495.
9. Ł. Otulakowski and B. Trzebicka, "Aggregation of Thermoresponsive Polymethacrylates in a Dulbecco's Modified Eagle Medium and Its Salts," *Polymers (Basel).*, 2023, doi: 10.3390/polym15173587.
10. Y. Raharjo *et al.*, "Dialysis Membranes for Acute Kidney Injury," 2022. doi: 10.3390/membranes12030325.
11. H. Ali *et al.*, "Visualizing subatomic orbital and spin moments using a scanning transmission electron microscope," *Nat. Mater.*, 2025, doi: 10.1038/s41563-025-02242-6.
12. J. Piscitelli *et al.*, "Clinical Evaluation of the Effect of Encorafenib on Bupropion, Rosuvastatin, and Coproporphyrin I and Considerations for Statin Coadministration," *Clin. Pharmacokinet.*, 2024, doi: 10.1007/s40262-024-01352-9.
13. S. Singh, H. Sharma, and S. Gohri, "A Comprehensive Review of the Synthesis , Characterization , and Antioxidant Potential of Phenothiazine Derivatives".
14. V. Chaudhary, A. P. Singh, H. Sharma, and D. Taumar, "The Role of Microglial Cells and Cytokine Modulation in Alzheimer ' s Disease : A Neuroinflammatory Perspective", doi: 10.2174/0115672050412712511150231 27.
15. G. Chen, Z. Y. Hu, Z. Guo, and Y. Xie, "Ultrafine Fe(OH)3 nanoparticles formation via oxidation-mediated strategies towards remarkable flame-retardant and smoke-suppressant performances," *Thermochim. Acta*, 2024, doi: 10.1016/j.tca.2024.179767.
16. S. A. Williams and M. E. French, "Effects of Dilatant Hardening on Fault Stabilization and Structural Development," *Geophys. Res. Lett.*, 2024, doi: 10.1029/2024GL108840.
17. L. Sun *et al.*, "Smart nanoparticles for cancer therapy," 2023. doi: 10.1038/s41392-023-01642-x.
18. Anantharapu Preethi Samyuktha, Yerikala Ramesh, Yadala Prapurna Chandra, and Venugopalaiah Penabaka, "A review of lyophilization," *GSC Biol. Pharm. Sci.*, 2025, doi: 10.30574/gscbps.2025.30.2.0035.
19. S. Bhattacharya, D. Singh, J. Aich, Ajazuddin, and M. B. Shete,

"Development and characterization of hyaluronic acid surface scaffolds Encorafenib loaded polymeric nanoparticles for colorectal cancer targeting," *Mater. Today Commun.*, 2022, doi: 10.1016/j.mtcomm.2022.103757.

20. M. Shi *et al.*, "The Intrinsic Role of Molecular Mass and Polydispersity Index in High-Performance Non-Fullerene Polymer Solar Cells," *Adv. Energy Mater.*, 2021, doi: 10.1002/aenm.202002709.
21. Y. Gong and L. Gu, "Transmission Electron Microscopy," in *Energy Storage Materials Characterization: Determining Properties and Performance: Volume 1-2*, 2025. doi: 10.1002/9783527834679.ch22.
22. R. Dummer *et al.*, "COLUMBUS 5-year update: a randomized, open-label, phase III trial of encorafenib plus binimetinib versus vemurafenib or encorafenib in patients with BRAF," 2023. doi: 10.2217/fon-2022-1258.
23. Y. Gong, X. Chen, and W. Wu, "Application of fourier transform infrared (FTIR) spectroscopy in sample preparation: Material characterization and mechanism investigation," *Adv. Sample Prep.*, 2024, doi: 10.1016/j.sampre.2024.100122.
24. P. Zambrano *et al.*, "Differential scanning calorimetry in drug-membrane interactions," 2024. doi: 10.1016/j.bbrc.2024.149806.
25. S. Fatimah, R. Ragadhita, D. F. Al Husaeni, and A. B. D. Nandiyanto, "How to Calculate Crystallite Size from X-Ray Diffraction (XRD) using Scherrer Method," *ASEAN J. Sci. Eng.*, 2022, doi: 10.17509/ajse.v2i1.37647.
26. M. Hadadian, R. Allahyari, B. Mahdavi, and M. Mohammadhosseini, "Comparative study of β-cyclodextrin and carboxymethyl-β-cyclodextrin as effective drug delivery systems for oxymetholone: Design, preparation, characterization, phase solubility and in vitro drug release studies," *J. Sci. Adv. Mater. Devices*, 2024, doi: 10.1016/j.jsamd.2024.100751.
27. L. Khalef, R. Lydia, K. Filicia, and B. Moussa, "Cell viability and cytotoxicity assays: Biochemical elements and cellular compartments," 2024. doi: 10.1002/cbf.4007.
28. B. N. Ikasari *et al.*, "Effect of Fetal Bovine Serum Concentration towards Vero Cells Growth on Culture in DMEM Medium," *J. Teknol. Lab.*, 2022, doi: 10.29238/teknolabjournal.v11i2.313.
29. Merck KGaA, "MTT Assay Protocol for Cell Viability and Proliferation," *Merck Gr.*, 2023.
30. A. P. Singh and T. S. Easwari, "Development and Characterization of Cinnamon Oil-Salicylic Acid Blended Nanoemulsion (CSN) for topical Application," *Indian J. Pharm. Educ. Res.*, vol. 56, no. 3, pp. S605–S612, 2022, doi: 10.5530/ijper.56.3s.169.
31. S. Forchhammer *et al.*, "Diagnosis of Basal Cell Carcinoma with Ex-vivo

Confocal Laser Scanning Microscopy in a Real-life Setting," *Acta Derm. Venereol.*, 2023, doi: 10.2340/actadv.v103.4859.

32. P. Álamo *et al.*, "Fluorescent dye labeling changes the biodistribution of tumor-targeted nanoparticles," *Pharmaceutics*, 2020, doi: 10.3390/pharmaceutics12111004.
33. M. Csidey *et al.*, "Examination of the Corneal Endothelium in Patients With Congenital Aniridia With a PAX6 Mutation Using In Vivo Confocal Laser Scanning Microscopy," *Cornea*, 2025, doi: 10.1097/ICO.0000000000003779.
34. Y. Y. Tyurina *et al.*, "Redox phospholipidomics discovers pro-ferroptotic death signals in A375 melanoma cells in vitro and in vivo," *Redox Biol.*, 2023, doi: 10.1016/j.redox.2023.102650.
35. V. Chaudhary, A. P. Singh, H. Sharma, D. Taumar, and I. Rajpoot, "Ophiocordyceps sinensis in Cancer Therapy : Bridging Traditional Medicine and Modern Oncology", doi: 10.2174/0115680266402650251110114152.
36. A. P. Singh, H. Sharma, D. Taumar, and I. Rajpoot, "Activities of Traditional Herbal Formulations : A Promising Adjunctive Approach for Respiratory Infections", doi: 10.2174/011573398X389387251125063114.
37. A. M. Menzies *et al.*, "POLARIS: A phase 2 trial of encorafenib plus binimetinib evaluating high-dose and standarddose regimens in patients with BRAF V600-mutant melanoma with brain metastasis," *Neuro-Oncology Adv.*, 2024, doi: 10.1093/noajnl/vdae033.
38. I. P. Sæbø, M. Bjørås, H. Franzyk, E. Helgesen, and J. A. Booth, "Optimization of the Hemolysis Assay for the Assessment of Cytotoxicity," *Int. J. Mol. Sci.*, 2023, doi: 10.3390/ijms24032914.